the two groups (patients with OCD vs healthy volunteers), were calculated. The paired *t* test was used to compare DT values for the CC regions between the patients with OCD and the matched control subjects. Because five comparisons were performed for each DT measure, *P* values lower than .01 were considered significant on the basis of Bonferroni correction. The correlations between DT measures of the CC regions studied and Y-BOCS and HDRS scores were investigated by using Spearman rank correlation coefficients. All statistical analyses were performed by using SPSS statistical software (SPSS for Windows, release 11.5 J; SPSS, Chicago, Ill).

Results

Our check of the raw echo-planar images for head motion revealed that the patients with OCD and the control subjects had kept equally still. The average superoinferior thickness of the rostrum measured in the sagittal plane for both groups was 6.875 mm. All intraclass correlation coefficients of DT measures were greater than 0.89 for every ROI, indicating excellent interoperator reliability.

There were no significant differences in D_M between the patients with OCD and the healthy volunteers (Table 1). A significant reduction in FA was observed in the CC rostrum of the patients with OCD compared with the rostral FA in the control subjects ($P < .001$). FA in the other subdivisions did not differ significantly between the patients and the healthy volunteers (Table 2). Higher FA in only the rostrum correlated significantly with lower Y-BOCS score ($r = -0.72$, $P = .002$) (Fig 3). HDRS score did not correlate with FA in the rostrum ($r = 0.06$, $P = .84$). Because none of the patients with OCD had an HDRS score higher than 7, we found noncorrelation between HDRS score and FA in the rostrum.

Discussion

Our study results indicate that in patients with OCD, there is abnormal white matter anisotropy in the rostrum of the CC and an inverse relationship between white matter anisotropy in the CC rostrum and severity of OCD symptoms. The reduced white matter anisotropy observed in our study suggests that patients with OCD possibly have microstructural abnormalities in the CC rostrum itself and fiber integrity abnormalities in the orbital prefrontal region that contains fibers extending into the rostrum. There is a large amount of experimental and clinical evidence that the OFC is involved in the mediation of emotional responses to biologically important stimuli (16). Results of animal studies suggest that hoarding, a common OCD symptom, is mediated by the ventromedial striatum, globus pallidus, and medial dorsal thalamus—all of which are connected to the OFC (16,24). Thus, heightened OFC activity may make individuals with OCD particularly efficient at recognizing conditioned aversive reinforcers and more vulnerable to anticipatory anxiety or distress (25). Since the OFC is involved in maintaining representations of the

Table 1

Mean Diffusivity for Selected Regions in Patients with OCD and Healthy Volunteers

Region	Mean Diffusivity*		*P* Value†	95% Confidence Interval‡
	Patients with OCD	Healthy Volunteers		
Rostrum	8.90 ± 2.28	7.74 ± 1.15	.15	−0.46, 2.78
Genu	8.10 ± 1.12	8.15 ± 1.01	.88	−0.88, 0.77
Rostral body	8.57 ± 1.32	7.93 ± 0.72	.12	−1.75, 1.44
Isthmus	9.09 ± 1.24	8.96 ± 1.00	.77	0.78, 1.04
Splenium	7.14 ± 0.81	7.12 ± 1.08	.88	−0.66, 0.57

* Mean diffusivity values ± standard deviations.

† $P < .01$ indicates significant difference on the basis of Bonferroni correction.

‡ Ninety-five percent confidence intervals for the difference in mean values between the patients and healthy volunteers.

Table 2

Mean FA Values for Selected Regions in Patients with OCD and Healthy Volunteers

Region	Mean FA*		*P* Value†	95% Confidence Interval‡
	Patients with OCD	Healthy Volunteers		
Rostrum	0.55 ± 0.07	0.69 ± 0.06	<.001	−1.18, −0.97
Genu	0.80 ± 0.07	0.81 ± 0.09	.70	−0.53, 0.36
Rostral body	0.68 ± 0.08	0.70 ± 0.06	.46	−0.66, 0.32
Isthmus	0.69 ± 0.08	0.73 ± 0.07	.06	−0.93, 0.01
Splenium	0.87 ± 0.10	0.86 ± 0.08	.74	−0.46, 0.63

* Mean FA values ± standard deviations.

† $P < .01$ indicate significant difference on the basis of Bonferroni correction.

‡ Ninety-five percent confidence intervals for the difference in mean values between the patients and healthy volunteers.

Figure 3

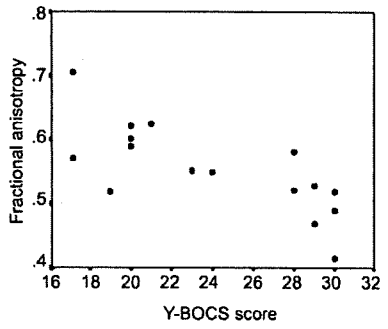

Figure 3: Graph illustrates relationship between Y-BOCS score and FA in CC rostrum of patients with OCD.

reinforcement value of stimuli in working memory, the inability of patients with this disorder to inhibit intrusive thoughts and images may be interpreted as reflective of a hyperactive working memory (26). The correlations between Y-BOCS score and white matter anisotropy of the CC rostrum that we observed suggest that white matter abnormalities in the orbitofrontal region are implicated in OCD symptom severity.

Szeszko et al (27) reported their use of DT imaging in patients with OCD. They compared, voxel by voxel, the imaging data in 15 patients with OCD and 15 healthy volunteers and observed substantially lower FA bilaterally in three areas of the anterior cingulated gyrus white matter in the patients with OCD. In our study, however, we chose an ROI analysis method aimed at identifying microstructural white matter abnormalities of the CC. The cingulum was not clearly defined in the transverse T2-weighted imaging planes, so we could not evaluate it. The contrasting findings of these two DT imaging studies may be due to differences in characteristics, such as age, sex, handedness, race, total Y-BOCS score, and/or HDRS score, between the patient groups. Furthermore, important group differences in the white matter integrity in other brain regions implicated in the pathophysiology of OCD, including the orbitofrontal lobe and striatal regions, were not observed in the Szeszko et al study (27).

We observed abnormal white matter FA in the CC rostrum of the patients with OCD. However, there were no significant differences in D_M between the groups. FA and D_M can be studied independently. FA is a measure of the directionality of diffusion. On the other hand, D_M is a measure of the average diffusion in all directions and thus is more sensitive to fiber density than to fiber orientation and organization (28). Although microstructural changes can be roughly estimated by using FA or D_M, both parameters are indispensable for yielding more pertinent information about morphologic changes in the brain. DT measures can be influenced by many factors, such as dense packing of axons, relative permeability of the membrane to water, internal axonal structure, tissue water content or degree of myelination, and/or the pathophysiology underlying the reduced white matter anisotropy. Although the pathophysiology underlying the reduced white matter anisotropy in the CC rostrum in patients with OCD has not been confirmed, more than one process may be responsible for the FA reduction.

Our study had limitations. A relatively small number of patients and control subjects were examined. There were also a few methodologic concerns. Because of the difficulty in placing ROIs in subcortical regions with no remarkable landmarks, microstructural abnormalities of the white matter tracts connecting the OFC to the rostrum were not directly examined. The Functool software applies thresholding to apparent diffusion coefficient maps that may substantially affect mean ROI data. Thus, the potential effects of medication on DT measures could not be examined. Also, since the source diffusion-weighted images had an in-plane spatial resolution of only 1.9 × 1.9 mm and a thickness of 4 mm, the noise introduced during the conversion of these images to FA maps could have limited the spatial resolution even further. We also cannot exclude the possibility that potential partial volume averaging effects influence DT measurements, especially in such a small subdivision of the CC as the rostrum, whose volume may differ between groups. However, for all subjects, the superoinferior thickness of the rostrum measured in the sagittal plane was 5–9 mm, greater than the 4-mm image section thickness. Furthermore, we cannot exclude the possibility that the head motion resulting from anxiety related to being inside the magnet differed between groups. Therefore, we checked the raw echo-planar images for head motion and verified that the patients with OCD and the control subjects had kept equally still.

In conclusion, our study results support the widely held view that the orbital prefrontal region is involved in the pathophysiology of OCD. It is important that the results also indicate that the OFC influences symptom severity in patients with OCD. Future studies with larger numbers of drug-naïve patients and more complex methods, such as tract tracing for direct examination of the targeted white matter, may help to elucidate the contribution of microstructural white matter changes in the orbitofrontal region to the pathophysiology and outcomes of OCD.

Acknowledgments: We are grateful to the MR imaging group at Kansai Medical University for valuable assistance.

References

1. Weissman MM, Bland RC, Canino GJ; for the Cross National Collaborative Group. The cross national epidemiology of obsessive compulsive disorder. J Clin Psychiatry 1994; 55(suppl):5–10.
2. Rasmussen SA, Eisen JL. The epidemiology and differential diagnosis of obsessive compulsive disorder. J Clin Psychiatry 1992; 53(suppl):4–10.
3. Dougherty DD, Rauch SL, Jenike MA. Pharmacotherapy for obsessive-compulsive disorder. J Clin Psychol 2004;60:1195–1202.
4. Purcell R, Maruff P, Kyrios M, Pantelis C. Cognitive deficits in obsessive-compulsive disorder on tests of frontal-striatal function. Biol Psychiatry 1998;43:348–357.
5. Greisberg S, McKay D. Neuropsychology of obsessive-compulsive disorder: a review and treatment implications. Clin Psychol Rev 2003;23:95–117.
6. Gazzaniga MS. Cerebral specialization and interhemispheric communication: does the corpus callosum enable the human condition? Brain 2000;123:1293–1326.
7. Pandya DN, Karol EA, Heilbronn D. The topographical distribution of interhemispheric projections in the corpus callosum of the rhesus monkey. Brain Res 1971;32: 31–43.
8. Barbas H, Pandya DN. Topography of commissural fibers of the prefrontal cortex in the rhesus monkey. Exp Brain Res 1984;55:187–191.
9. Seltzer B, Pandya DN. The distribution of posterior parietal fibers in the corpus callosum of the rhesus monkey. Exp Brain Res 1983;49:147–150.
10. de Lacoste MC, Kirkpatrick JB, Ross ED. Topography of the human corpus callosum. J Neuropathol Exp Neurol 1985;44:578–591.
11. Abe O, Masutani Y, Aoki S, et al. Topography of the human corpus callosum using dif-

fusion tensor tractography. J Comput Assist Tomogr 2004;28:533–539.

12. Baxter LR Jr, Phelps ME, Mazziotta JC, Guze BH, Schwartz JM, Selin CE. Local cerebral glucose metabolic rates in obsessive-compulsive disorder: a comparison with rates in unipolar depression and in normal controls. Arch Gen Psychiatry 1987;44:211–218.
13. Swedo SE, Schapiro MB, Grady CL, et al. Cerebral glucose metabolism in childhood-onset obsessive-compulsive disorder. Arch Gen Psychiatry 1989;46:518–523.
14. Rauch SL, Jenike MA, Alpert NM, et al. Regional cerebral blood flow measured during symptom provocation in obsessive-compulsive disorder using oxygen 15-labeled carbon dioxide and positron emission tomography. Arch Gen Psychiatry 1994;51:62–70.
15. Baxter LR Jr, Schwartz JM, Bergman KS, et al. Caudate glucose metabolic rate changes with both drug and behavior therapy for obsessive-compulsive disorder. Arch Gen Psychiatry 1992;49:681–689.
16. Zald DH, Kim SW. Anatomy and function of the orbital frontal cortex. I. Anatomy, neurocircuitry, and obsessive-compulsive disorder. J Neuropsychiatry Clin Neurosci 1996; 8:125–138.
17. Basser PJ, Pierpaoli C. Microstructural and physiological features of tissues elucidated by quantitative-diffusion-tensor MRI. J Magn Reson B 1996;111:209–219.
18. Lim KO, Hedehus M, Moseley M, de Crespigny A, Sullivan EV, Pfefferbaum A. Compromised white matter tract integrity in schizophrenia inferred from diffusion tensor imaging. Arch Gen Psychiatry 1999;56:367–374.
19. Minami T, Nobuhara K, Okugawa G, et al. Diffusion tensor magnetic resonance imaging of disruption of regional white matter in schizophrenia. Neuropsychobiology 2003; 47:141–145.
20. Okugawa G, Nobuhara K, Minami T, et al. Subtle disruption of the middle cerebellar peduncles in patients with schizophrenia. Neuropsychobiology 2004;50:119–123.
21. Nobuhara K, Okugawa G, Sugimoto T, et al. Frontal white matter anisotropy and symptom severity of late-life depression: a magnetic resonance diffusion tensor imaging study. J Neurol Neurosurg Psychiatry 2006; 77:120–122.
22. American Psychiatric Association. Diagnostic and statistical manual of mental disorders, 4th ed. Washington, DC: American Psychiatric Association, 2000; 456–462.
23. Witelson SF, Kigar DL. Anatomical development of corpus callosum in humans: a review with reference to sex and cognition. In: Molefese DL, Segalowitz SJ, eds. Brain lateralization in children: development implications. New York, NY: Guilford, 1988; 35–37.
24. Mogenson GJ, Wu M. Disruption of food hoarding by injections of procaine into mediodorsal thalamus, GABA into subpallidal region and haloperidol into accumbens. Brain Res Bull 1988;20:247–251.
25. Zald DH, Kim SW. Anatomy and function of the orbital frontal cortex. II. Function and relevance to obsessive-compulsive disorder. J Neuropsychiatry Clin Neurosci 1996;8: 249–261.
26. Goldman-Rakic PS. Circuitry of primate prefrontal cortex and regulation of behavior by representational memory. In: Plum F, Mountcastle V, eds. Handbook of physiology: the nervous system. Bethesda, Md: American Physiological Society, 1987; 373–417.
27. Szeszko PR, Ardekani BA, Ashtari M, et al. White matter abnormalities in obsessive-compulsive disorder: a diffusion tensor imaging study. Arch Gen Psychiatry 2005;62: 782–790.
28. Kubicki M, Westin CF, Nestor PG, et al. Cingulate fasciculus integrity disruption in schizophrenia: a magnetic resonance diffusion tensor imaging study. Biol Psychiatry 2003;54:1171–1180.

Cardiovasc Intervent Radiol (2008) 31:332–335
DOI 10.1007/s00270-007-9246-8

CLINICAL INVESTIGATION

Biochemical Markers of Bone Turnover in Percutaneous Vertebroplasty for Osteoporotic Compression Fracture

Atsushi Komemushi · Noboru Tanigawa · Shuji Kariya · Hiroyuki Kojima · Yuzo Shomura · Takanori Tokuda · Motoo Nomura · Jiro Terada · Minoru Kamata · Satoshi Sawada

Received: 17 July 2007 / Accepted: 9 November 2007 / Published online: 12 December 2007

Abstract
Purpose To evaluate relationships between biochemical markers of bone turnover, bone mineral density, and new compression fractures following vertebroplasty.
Methods Initially, we enrolled 30 consecutive patients with vertebral compression fractures caused by osteoporosis. Twenty-three of the 30 patients visited our hospital for follow-up examinations for more than 4 weeks after vertebroplasty. The patients were divided into two groups: patients with new fractures (group F) and patients with no new fractures (group N). We analyzed differences in the following parameters between these two groups: serum bone alkaline phosphatase, urinary crosslinked N-telopeptide of type I collagen, urinary deoxypyridinoline, and bone mineral density. Next, the patients were divided into another two groups: patients with higher risk (group H: urinary cross-linked N-telopeptide of type I collagen >54.3 nmol BCE/mmol Cr or urinary deoxypyridinoline >7.6 nmol/mmol Cr, and serum bone alkaline phosphatase <29.0 U/l) and patients with lower risk (group L). We analyzed the difference in the rate of new fractures between these two groups.
Results We identified 9 new fractures in 7 patients. There were no significant differences between groups F and N. We identified 5 new fractures in 3 of the 4 patients in group H, and 4 new fractures in 4 of the 19 patients in group L. There was a significant difference in the rate of new fractures between groups H and L.
Conclusions A combination of high levels of bone resorption markers and normal levels of bone formation markers may be associated with increased risk of new recurrent fractures after percutaneous vertebroplasty.

Keywords Interventional radiology · Osteoporosis · Spine · Vertebral fracture · Vertebroplasty

A. Komemushi (✉) · N. Tanigawa · S. Kariya · H. Kojima · Y. Shomura · T. Tokuda · M. Nomura · J. Terada · M. Kamata · S. Sawada
Department of Radiology, Kansai Medical University, 2-3-1 Shinmachi, Hirakata, Osaka 573-1191, Japan
e-mail: kome64@yo.rim.or.jp

Introduction

Percutaneous vertebroplasty is used to treat back pain caused by compression fractures. Injecting bone cement into fractured vertebral bodies increases the strength and stability of vertebral body bone, which is thought to be a factor in alleviation of pain [1–3]. Several studies indicate that new fractures can occur following percutaneous vertebroplasty [4–7]. Osteoporosis, which is a skeletal disorder characterized by decreased bone strength that increases the risk of fracture, affects the occurrence of new fractures after vertebroplasty [3–5]. Bone strength is determined by bone mineral density and bone quality [8]. Bone quality is determined by characteristics of the bone matrix, such as microarchitecture, bone turnover, microdamage accumulation, the degree of calcification, and collagen [9, 10]. Currently, it is thought that the only reliable way to clinically assess bone quality is to characterize bone metabolism by assaying biochemical markers of bone turnover [8]. The present study evaluated relationships between biochemical markers of bone turnover, bone mineral density, and new compression fractures following vertebroplasty.

Patients and Methods

This study was approved by our Institutional Review Board. All patients received explanations of the

percutaneous vertebroplasty and the handling of clinical data, and written informed consent was obtained from each patient. There was no financial relationship between the investigators and the study subjects.

Initially, we enrolled 30 consecutive patients with vertebral body compression fractures caused by osteoporosis. All patients underwent percutaneous vertebroplasty at a single institution from January 2005 to December 2005. Patients with traumatic compression fracture or malignant tumors were excluded from this study. The latest clinical data we used were obtained in September 2006. Twenty-three of the 30 patients visited our hospital for follow-up examinations for more than 4 weeks after vertebroplasty (mean follow-up term, 255.0 ± 173.1 days; median follow-up term, 275.5 days; range, 31–591 days). These 23 patients (21 women, 2 men; mean age, 72.1 ± 6.7 years; age range, 63–86 years), encompassing 48 vertebral body compression fractures (Th6, 1; Th7, 3; Th8, 2; Th9, 4; Th10, 3; Th11, 8; Th12, 6; L1, 7; L2, 4; L3, 9; L4, 1), and 26 percutaneous vertebroplasty procedures, were the subjects of this study.

The indication for vertebroplasty was compression fracture causing significant back pain that was not relieved by conservative treatment. Patients underwent the following numbers of vertebroplasty procedures: one procedure, 20 patients; two procedures, 3 patients. Before each vertebroplasty procedure, we measured serum bone alkaline phosphatase, urinary crosslinked N-telopeptide of type I collagen, urinary deoxypyridinoline, and bone mineral density. Bone mineral density of the second metacarpal bone was measured by computed X-ray densitometry (Bonalyzer II, Teijin, Tokyo, Japan), and the quantity ΣGS/D (mmAl) was used for analysis.

Percutaneous vertebroplasty was performed in an angiography room with an IVR-CT system (Advantex LCA + ACT, GE Medical Systems, Milwaukee, WI, USA), which combines angiographic equipment and CT equipment with a single fluoroscopy table. After intramuscular injection of 25 mg of hydroxyzine hydrochloride (Atarax P, Pfizer Japan, Tokyo, Japan), 0.5 mg of atropine sulfate (Tanabe Seiyaku, Osaka, Japan) and 10 mg of morphine hydrochloride (Sankyo, Tokyo, Japan), the patient was placed prone on the fluoroscopy table. The skin, subcutaneous tissues, and periosteum over the pedicle to be punctured were anesthetized with 1% lidocaine hydrochloride (Xylocaine polyamp 1%, AstraZeneca, Osaka, Japan). A 13G needle (Osteo-Site Bone Biopsy Needle Murphy M2; length, 10 cm; Cook, Bloomington, IN, USA) was advanced until its tip penetrated the cortex, with reference to CT images. With lateral fluoroscopic guidance, the needle was advanced into the vertebral body. Ideally, the tip of the needle was placed in the anterior third of the vertebral body, close to the midline. More posterior needle positions were sometimes necessary when treating severely compressed vertebral bodies with steep pedicle angulation.

Intraosseous venography was performed with 10–20 ml of CO_2 to confirm that the needle was not positioned within a direct venous anastomosis to the central or epidural veins [11]. Then, 20 g of methylmethacrylate powder (Osteobond copolymer bone cement; Zimmer, Warsaw, IN, USA) was mixed with 5 g of barium sulfate powder (Horii Pharmaceutical, Osaka, Japan) that had been sterilized with dry heat to increase its opacity [12]. Next, 10 ml of liquid methylmethacrylate monomer was added to the powder, and the mixture was blended to a toothpaste-like consistency, producing polymethylmethacrylate (PMM). Using 1 ml syringes, the PMM was injected with lateral fluoroscopic guidance. PMM injection was terminated when adequate filling of the vertebral body was achieved, or if leakage occurred. If leakage occurred, the needle was repositioned, and additional PMM was injected to fill the remaining part of the vertebral body. After the needle was removed, all patients were observed in a supine position for 2 hr.

After the vertebroplasty, the patients were followed up with physical examinations and radiographs at 1 to 3 days and 1, 4, 10, and 22 months after vertebroplasty, and if back pain relapsed. If a patient did not visit the hospital for follow-up, a physician telephoned them to encourage them to visit. Even if no new fractures were observed on radiographs, MRI was performed to check for microfractures or incomplete fractures if new fractures were suspected on physical examination. MRI was performed using a 1.5 T MRI system (Signa Horizon LX software version 9.1; General Electric Medical Systems, Milwaukee, WI, USA) and a phased-array cervico-thoraco-lumbar coil. At all MRI examinations, images were acquired using the following procedures: T1-weighted fast gradient echo (TR, 10 msec; TE, 4 msec; flip angle, 30°); sagittal T1-weighted spin echo (TR, 500 msec; TE, 9 msec; excitations, 4; matrix, 384 × 256); and sagittal T2-weighted fast spin echo with fat suppression (TR, 4000 msec; TE, 102 msec; excitations, 2; matrix, 320 × 256). Additional imaging procedures were performed if necessary. The criteria for diagnosis of vertebral fracture were deformation of the vertebral body on plain radiographs and a change in vertebral signal intensity on MRI [13]. We recommended to all patients that they be administered vitamin D or antiresorptive agents by their family doctor.

The patients were divided into two groups: patients with new fractures (group F) and patients with no new fractures (group N). Using Student's *t*-test, we analyzed differences in the following parameters between these two groups: serum bone alkaline phosphatase, urinary crosslinked N-telopeptide of type I collagen, urinary deoxypyridinoline, and bone mineral density.

Next, the patients were divided into another two groups: patients with higher risk of fracture (group H) and patients with lower risk of fracture (group L). Group H was defined according to guidelines for the use of biochemical markers of bone turnover in osteoporosis [8]: urinary crosslinked N-telopeptide of type I collagen >54.3 nmol BCE/mmol Cr or urinary deoxypyridinoline >7.6 nmol/mmol Cr; and serum bone alkaline phosphatase <29.0 U/l. Using the chi-square test, we analyzed the difference in the rate of new fractures between group H and group L.

A probability value of $p < 0.05$ was considered significant. All analyses were performed using StatView for Windows (version 5.0, SAS Institute, Cary, NC, USA).

Results

We identified 9 new fractures in 7 (30%) of the 23 patients. These 7 patients comprised group F. The remaining 16 patients (70%) comprised group N.

In group F and group N, respectively, serum bone alkaline phosphatase was 30.1 ± 15.3 and 25.3 ± 8.6 U/l, urinary crosslinked N-telopeptide of type I collagen was 63.9 ± 33.2 and 50.7 ± 29.2 nmol BCE/mmol Cr, urinary deoxypyridinoline was 8.4 ± 2.9 and 7.3 ± 3.3 nmol/mmol Cr, and bone mineral density was 2.2 ± 0.2 and 2.0 ± 0.3 mmAl. There were no significant differences in bone mineral density or any of the biochemical markers of bone turnover that we evaluated between group F and group N (Table 1). There was no significant difference in age, gender, locations, and activity after initial vertebroplasty between group F and group N.

Group H comprised 4 (17%) of the 23 patients, and group L comprised the remaining 19 patients (83%). We identified 5 new fractures in 3 (75%) of the 4 patients in group H, and 4 new fractures in 4 (21%) of the 19 patients in group L. There was a significant difference in the rate of new fractures between group H and group L (chi-square test: $p = 0.03$) (Table 2). There was no significant difference in age, gender, locations, and activity after initial vertebroplasty between group H and group L.

Table 2 Comparison of occurrence of new fractures between group H (high fracture risk) and group L (low fracture risk)

	New fractures	No new fractures	Total
Group H ($n = 4$)	3	1	4
Group L ($n = 19$)	4	15	19
Total	7	16	23

Group H: urinary crosslinked N-telopeptide of type I collagen >54.3 nmol BCE/mmol Cr or urinary deoxypyridinoline > 7.6, and serum bone alkaline phosphatase < 29.0 U/l

Chi-square test: $p = 0.03$

Discussion

There have been reports of new vertebral fractures following percutaneous vertebroplasty [4–6]. New vertebral fractures are 5 times more likely to occur in patients with compression fractures caused by osteoporosis, but it is unclear whether these fractures are due to the natural history of osteoporosis or the effects of vertebroplasty [14, 15]. When following patients after percutaneous vertebroplasty, it is important to be able to predict the risk of new vertebral fractures. It is thought that various factors are involved in the occurrence of new fractures after vertebroplasty [16]. In the present study, we examined relationships between bone mineral density, biochemical markers of bone turnover, and new fractures after vertebroplasty.

In several previous studies of new fractures after vertebroplasty [5, 6], follow-up examinations were performed when symptoms recurred; consequently, researchers were unable to detect asymptomatic vertebral fractures. In the present study, the patients were followed whether or not symptoms recurred, allowing us to identify asymptomatic vertebral fractures. Furthermore, whereas incomplete fractures are difficult to identify on spine radiographs, they can easily be seen on MRI scans. In a previous study, 67% of new compression fractures following percutaneous vertebroplasty occurred within 30 days after the surgery [5]. In the present study, we found 9 new fractures in 7 (30%) of the 23 consecutive patients, who were followed

Table 1 Comparison of the following parameters between groups F (new fractures) and N (no new fractures): serum bone alkaline phosphatase, urinary crosslinked N-telopeptide of type I collagen, urinary deoxypyridinoline, and bone mineral density

	Group F ($n = 7$)	Group N ($n = 16$)	Student's t-test
Serum bone alkaline phosphatase (U/l)	30.1 ± 15.3	25.3 ± 8.6	NS
Urinary crosslinked N-telopeptide of type I collagen (nmol BCE/mmol Cr)	63.9 ± 33.2	50.7 ± 29.2	NS
Urinary deoxypyridinoline (nmol/mmol Cr)	8.4 ± 2.9	7.3 ± 3.3	NS
Bone mineral density (mmAl)	2.2 ± 0.2	2.0 ± 0.3	NS

for more than 4 weeks, with an average follow-up period of 255.0 days.

As the bone mineral density of trunk bones can be affected by compression fractures or bone cement, the bone mineral density of the second metacarpal bone was measured in this study. Previous meta-analysis of bone mineral density and risk of vertebral fractures indicates that the confidence intervals for estimates of relative risk of new vertebral fractures are relatively wide in the great majority of trials. The meta-analysis showed that a 1% improvement in bone mineral density was associated with a 0.03 decrease in the relative risk of vertebral fractures, and indicated that the status of bone resorption is more predictive than bone mineral density [17]. In the present study, serum bone alkaline phosphatase was measured as a bone formation marker. Bone formation markers are directly or indirectly produced by osteoblasts during bone development [8]. In the present study, urinary crosslinked N-telopeptide of type I collagen and urinary deoxypyridinoline were measured as bone resorption markers. Bone resorption markers are produced by osteoclasts during bone resorption, and a decrease in these markers indicates a reduction in the risk of fracture [8]. We did not find any differences in any of the biochemical markers of bone turnover or bone mineral density between group F and group N.

According to the Japan Osteoporosis Society's Guidelines, a combination of high levels of bone resorption markers and normal levels of bone formation markers is associated with a higher risk of fracture [8]. We divided the present patients into two groups: higher risk of fracture (group H) and lower risk of fracture (group L). Group H was defined according to guidelines for the use of biochemical markers of bone turnover in osteoporosis: urinary crosslinked N-telopeptide of type I collagen >54.3 nmol BCE/mmol Cr or urinary deoxypyridinoline >7.6 nmol/mmol Cr, and serum bone alkaline phosphatase <29.0 U/l. Group H had a significantly higher incidence rate of fracture than group L.

The present study had the following limitations: the study group comprised a relatively small number of patients (in particular there were only 4 patients in group H) treated at a single institution, and subjects received antiresorptive drugs or vitamin D that were administered by their family doctor which were not controlled by the researchers.

In conclusion, this single-center feasibility study suggests a relationship between high levels of bone resorption markers and normal levels of bone formation markers and an increased risk of new recurrent fractures after percutaneous vertebroplasty. These findings may warrant validation a larger prospective multicenter study.

References

1. Cotten A, Boutry N, Cortet B et al. (1998) Percutaneous vertebroplasty: State of the art. Radiographics 18:311–323
2. Peh WC, Gilula LA, Peck DD (2002) Percutaneous vertebroplasty for severe osteoporotic vertebral body compression fractures. Radiology 223:121–126
3. Kallmes DF, Jensen ME (2003) Percutaneous vertebroplasty. Radiology 229:27–36
4. Grados F, Depriester C, Cayrolle G et al. (2000) Long-term observations of vertebral osteoporotic fractures treated by percutaneous vertebroplasty. Rheumatology (Oxford) 39:1410–1414
5. Uppin AA, Hirsch JA, Centenera LV et al. (2003) Occurrence of new vertebral body fracture after percutaneous vertebroplasty in patients with osteoporosis. Radiology 226:119–124
6. Lin EP, Ekholm S, Hiwatashi A et al. (2004) Vertebroplasty: Cement leakage into the disc increases the risk of new fracture of adjacent vertebral body. AJNR Am J Neuroradiol 25:175–180
7. Komemushi A, Tanigawa N, Kariya S et al. (2006) Percutaneous vertebroplasty for osteoporotic compression fracture: Multivariate study of predictors of new vertebral body fracture. Cardiovasc Intervent Radiol 29:580–585
8. Nishizawa Y, Nakamura T, Ohta H et al. (2005) Guidelines for the use of biochemical markers of bone turnover in osteoporosis (2004). J Bone Miner Metab 23:97–104
9. Weinstein RS (2000) True strength. J Bone Miner Res 15:621–625
10. Chesnut CH 3rd, Rosen CJ, Bone Quality Discussion Group (2001) Reconsidering the effects of antiresorptive therapies in reducing osteoporotic fracture. J Bone Miner Res 16:2163–2172
11. Tanigawa N, Komemushi A, Kariya S et al. (2005) Intraosseous venography with carbon dioxide contrast agent in percutaneous vertebroplasty. AJR Am J Roentgenol 184:567–570
12. Leibold RA, Gilula LA (2002) Sterilization of barium for vertebroplasty: An effective, reliable, and inexpensive method to sterilize powders for surgical procedures. AJR Am J Roentgenol 179:198–200
13. Maehara M, Tanigawa N, Ikeda K et al. (2006) Gadolinium-enhanced magnetic resonance imaging after percutaneous vertebroplasty does not improve the short-term prediction of new compression fractures. Acta Radiol 47:817–822
14. Lindsay R, Silverman SL, Cooper C et al. (2001) Risk of new vertebral fracture in the year following a fracture. JAMA 285:320–323
15. Delmas PD, Ensrud KE, Adachi JD et al. (2002) Multiple Outcomes of Raloxifene Evaluation Investigators. Efficacy of raloxifene on vertebral fracture risk reduction in postmenopausal women with osteoporosis: Four-year results from a randomized clinical trial. J Clin Endocrinol Metab 87:3609–3617
16. Hulme PA, Krebs J, Ferguson SJ et al. (2006) Vertebroplasty and kyphoplasty: A systematic review of 69 clinical studies. Spine 31:1983–2001
17. Cummings SR, Karpf DB, Harris F et al. (2002) Improvement in spine bone density and reduction in risk of vertebral fractures during treatment with antiresorptive drugs. Am J Med 112:281–289

ORIGINAL ARTICLE

ACTA RADIOLOGICA

Diffusion-Weighted Imaging for Predicting New Compression Fractures Following Percutaneous Vertebroplasty

T. SUGIMOTO, N. TANIGAWA, K. IKEDA, N. OHMURA, M. MAEHARA, S. KARIYA, H. KOJIMA, A. KOMEMUSHI, S. K. HA-KAWA, Y. SAITO, A. TAJIKA, T. KINOSHITA & S. SAWADA

Department of Radiology and Department of Neuropsychiatry, Kansai Medical University Takii Hospital, Osaka, Japan; Department of Radiology, Kansai Medical University, Osaka, Japan

Sugimoto T, Tanigawa N, Ikeda K, Ohmura N, Maehara M, Kariya S, Kojima H, Komemushi A, Ha-Kawa SK, Saito Y, Tajika A, Kinoshita T, Sawada S. Diffusion-weighted imaging for predicting new compression fractures following percutaneous vertebroplasty. Acta Radiol 2008;49:419–426.

Background: Percutaneous vertebroplasty (PVP) is a technique that structurally stabilizes a fractured vertebral body. However, some patients return to the hospital due to recurrent back pain following PVP, and such pain is sometimes caused by new compression fractures.

Purpose: To investigate whether the apparent diffusion coefficient (ADC) of adjacent vertebral bodies as assessed by diffusion-weighted imaging before PVP could predict the onset of new compression fractures following PVP.

Material and Methods: 25 patients with osteoporotic compression fractures who underwent PVP were enrolled in this study. ADC was measured for 49 vertebral bodies immediately above and below each vertebral body injected with bone cement before and after PVP. By measuring ADC for each adjacent vertebral body, ADC was compared between vertebral bodies with a new compression fracture within 1 month and those without new compression fractures. In addition, the mean ADC of adjacent vertebral bodies per patient was calculated.

Results: Mean preoperative ADC for the six adjacent vertebral bodies with new compression fractures was 0.55×10^{-3} mm^2/s (range 0.36–1.01 $\times 10^{-3}$ mm^2/s), and for the 43 adjacent vertebral bodies without new compression fractures 0.20×10^{-3} mm^2/s (range 0–0.98 $\times 10^{-3}$ mm^2/s) ($P < 0.001$). Mean preoperative ADC for the six patients with new compression fractures was 0.55×10^{-3} mm^2/s (range 0.21–1.01 $\times 10^{-3}$ mm^2/s), and that for the 19 patients without new compression fractures 0.17×10^{-3} mm^2/s (range 0.01–0.43 $\times 10^{-3}$ mm^2/s) ($P < 0.001$).

Conclusion: The ADC of adjacent vertebral bodies as assessed by diffusion-weighted imaging before PVP might be one of the predictors for new compression fractures following PVP.

Key words: Adults; CNS; MR diffusion; spine; vertebroplasty

Tatsuya Sugimoto, Department of Radiology and Neuropsychiatry, Kansai Medical University Takii Hospital, 10–15 Fumizono, Moriguchi, Osaka, 570-8507, Japan (tel. +81 6 6992 1001, fax. +81 6 6995 2669, e-mail. sugimota@takii.kmu.ac.jp)

Accepted for publication December 6, 2007

Percutaneous vertebroplasty (PVP) was introduced into the literature in 1987 (1). Since then, PVP has been performed to treat back pain associated with vertebral body compression fractures caused by various factors, and is now widely performed due to its drastic pain-relieving effects. PVP is a technique that structurally stabilizes a fractured vertebral body by injecting a self-curing cement substance that uses polymethyl methacrylate (PMMA) as the main component. However, some patients return to the hospital due to recurrent back pain following PVP. Such pain is sometimes caused by new compression fractures. While general consensus is lacking regarding the causes of new compression fractures following PVP, new fractures often occur in vertebral bodies adjacent to the vertebral bodies treated by PVP (2–4). Furthermore, such new compression fractures occur relatively

informa
healthcare

DOI 10.1080/02841850801886109

soon after PVP (4). If new adjacent-level compression fractures can be predicted prior to PVP, use of prophylactic PVP in adjacent vertebral bodies may be justified (5–9).

In recent years, many studies have investigated the differentiation between benign and malignant compression fractures using diffusion-weighted magnetic resonance imaging (MRI) (10–14). Diffusion-weighted imaging (DWI) allows visualization of the diffusion of water molecules exhibiting random and Brownian motions in tissue, and ascertainment of microscopic findings for cells. Furthermore, measuring the apparent diffusion coefficient (ADC) allows objective assessment of diffusion. In an attempt to establish the possibility of prophylactic PVP, the present study examined vertebral bodies adjacent to vertebral bodies injected with bone cement substance, based on the hypothesis that adjacent vertebrae are at high risk of compression fractures. The purpose of this study was to ascertain whether the ADC of adjacent vertebral bodies as assessed by diffusion-weighted imaging prior to PVP could predict the onset of new compression fractures following PVP.

Material and Methods

This study was approved by the institutional review board. All patients provided written informed consent.

Patients

The subjects in this study comprised 31 (27 female, four male; mean age 71.2±8.4 years, range 44–84 years) consecutive patients who underwent PVP for vertebral compression fractures resulting from osteoporosis between April and July 2003. Indication for PVP was back pain caused by compression fracture of a vertebral body with pain on percussion of the vertebral spinous process. In cases with multiple compression fractures in which percussion pain of spinous process was unclear, physical examination was performed using fluoroscopy. Patients with back pain attributed to myelopathy or radiculopathy resulting from stenosis of the vertebral canal or narrowing of the intervertebral foramen were excluded from the present study. Examinations performed before the procedure comprised physical and neurological examinations, electrocardiography, respiratory function testing, laboratory investigations, evaluation of back pain using visual analogue scale (VAS) score and the following diagnostic imaging studies: anterior and lateral radiographs of the thoracic and lumbar vertebrae, MRI of the spine, including the vertebra affected by the compression fracture, and computed tomography (CT).

ADC was measured for the vertebral bodies immediately above and below each vertebral body injected with bone cement. Inclusion and exclusion criteria were as follows. Vertebrae placed just below and above the treated vertebrae and where ADC could be accurately calculated were included in our study. The following vertebrae were excluded: vertebrae injected with bone cement after initial PVP within 1 month; first sacrum (S1); fractured vertebrae; vertebrae with susceptibility artifacts. A patient summary, including excluded patients, is shown in Table 1.

PVP was performed on 69 vertebral bodies. Six patients were excluded due to the reasons listed in Table 1. The remaining 25 patients (22 female, three male; mean age 72.2±6.5 years, range 54–84 years) were included in the final analysis. A total of 56 vertebral bodies (20 thoracic vertebral bodies and 36 lumbar vertebral bodies) were treated by PVP in these 25 patients. The number of treated vertebral bodies was one in seven patients, two in seven patients, three in nine patients, and four in two patients. Among the 18 patients in whom cement injection was performed in multiple vertebral bodies, the number of normal vertebral bodies between treated vertebral bodies was zero in nine patients, one in three patients, two in five patients, and three in one patient. Thus, excluding S1, a total of 62 adjacent vertebral bodies were examined. Of the 62 vertebral bodies, four vertebral bodies with compression fractures identified at the time of PVP and nine vertebral bodies in which ADC could not be measured due to susceptibility artifacts were excluded. ADC was thus measured in 49 vertebral bodies (16 thoracic vertebral bodies, 33 lumbar vertebral bodies).

MR imaging protocol

MRI was performed using a 1.5T MRI system (Signa Horizon LX software version 9.1; GE HealthCare, Milwaukee, Wisc., USA) within 3 days before PVP and within 1 week after PVP. A quadrature detection thoracolumbar spine coil was used for T1- and T2-weighted imaging and DWI. Following T1-weighted fast gradient-echo coronal localizer images, sagittal T1-weighted spin-echo (TR/TE 675/12 ms, slice thickness 3.7 mm, intersection gap 0.8 mm, field of view [FOV] 30 × 30 cm, matrix size 384 × 256, echo train length 4) and sagittal T2-weighted fast spin-echo with fat suppression (TR/TE 4000/102 ms, slice thickness 3.7 mm,

Table 1. Patient data.

Patient	Sex	Age, years	PVP performed on vertebral bodies	Adjacent vertebral bodies	Analyzed vertebral bodies	Reason for analysis exclusion
A	M	76	L2, L3	L1, L4	L1, L4	
B	F	66	TH12, L1, L2, L3	Th11, L4	Th11, L4	
C	F	74	Th11, Th12, L1	Th10, L2	Th10, L2	
D	F	76	Th6, Th8	Th5, Th7, Th9	Th9	Th5: artifacts Th7: artifacts
E	F	79	Th12	Th11, L1	Th11, L1	
F	M	66	L1	Th12, L2	Th12, L2	
G	M	54	L1	Th12, L2	Th12, L2	
H	F	70	Th12	Th11, L1	Th11, L1	
I	F	69	Th12, L1, L2	Th11, L3	Th11, L3	
J	F	64	L1, L2	Th12, L3	L3	Th12: artifacts
K	F	80	Th12, L3	Th11, L1, L2, L4	L1	Th11: artifacts L2: compression fracture L4: compression fracture
L	F	76	L1, L4	Th12, L2, L3, L5	L2, L3, L5	Th12: artifacts
M	F	69	Th12, L1, L3	Th11, L2, L4	L2, L4	Th11: artifacts
N	F	72	L3	L2, L4	L2, L4	
O	F	70	L4, L5	L3	L3	
P	F	71	L1, L2, L3	Th12, L4	Th12, L4	
Q	F	84	L3	L2, L4	L2, L4	
R	F	76	Th11, Th12, L1, L2	Th10, L3	Th10	L3: compression fracture
S	F	78	L1, L4, L5	Th12, L2, L3	Th12, L2, L3	
T	F	63	Th12	Th11, L1	Th11, L1	
U	F	79	Th11, Th12, L3	Th10, L1, L2, L4	L1, L2, L4	Th10: artifacts
V	F	71	Th12, L4, L5	Th11, L1, L3	Th11, L3	L1: compression fracture
W	F	71	Th12, L1, L3	Th11, L2, L4	Th11, L2, L4	
X	F	78	Th9, Th12, L1	Th8, Th10, Th11, L2	Th11, L2	Th8: artifacts Th10: artifacts
Y	F	74	Th12, L1	Th11, L2	Th11, L2	
($n=25$)	3 M, 22 F	72.2±6.5	56 (20 Th, 36 L)	62 (25 Th, 37 L)	49 (16 Th, 33 L)	13 (9 Th, 4 L)
Excluded patients						
a	M	84	L3, L4, L5			L2: compression fracture
b	F	59	L3, L4, L5			Additional PVP was performed 6 days after initial PVP
c	F	74	L2			Additional PVP was performed 6 days after initial PVP
d	F	72	Th12			Th11 and L1: artifact
e	F	69	Th11, Th12			Additional PVP was performed 7 days after initial PVP
f	F	44	Th10, Th11, Th12			Th9 and L1: compression fracture
($n=6$)			13 (3 Th, 7 L)			

intersection gap 0.8 mm, FOV 30 × 30 cm, matrix size 320 × 256, echo train length 16) images were acquired. The MR pulse sequence used for DWI was a single-shot echo-planar pulse sequence with fat saturation (TR/TE 5000/99.1 ms, receiver bandwidth ±108 kHz, FOV 30 × 30 cm, matrix size 128 × 128, slice thickness 8 mm, interslice gap 2 mm, number of excitations [NEX] 1). Using these parameters, seven sagittal diffusion-weighted images were acquired.

ADCs were calculated with only two *b* factors (0 s/mm^{-2}, 1000 s/mm^{-2}) (two-point technique) (15).

Data from DWI were transferred to a GE Advantage Workstation 3.1, where ADCs were calculated using a subprogram of the Functool2 image analysis software (GE HealthCare, Buc, France). A user-defined region of interest (ROI) was placed in the mid-sagittal diffusion-weighted image. On the target vertebral bodies, the large

fitting circle or ellipse was positioned centrally (Fig. 1). Special care was taken to avoid cerebrospinal fluid signal or vertebral disk signal. The average ADC within the ROI calculated by Functool2 was presumed to be the mean ADC of the target vertebral body.

Follow-up protocol and outcome evaluation

Frontal and lateral radiographs of the thoracic and lumbar vertebrae were performed within 3 days of PVP (baseline). At 1 month after PVP, a frontal and lateral radiograph of the thoracic and lumbar vertebrae was performed, in addition to MRI. Subjects were instructed to return to the hospital if back pain recurred within 1 month of PVP, and frontal and lateral radiographs of the thoracic and lumbar vertebrae and MRI were taken at this point in time. VAS was used for the evaluation of back pain. New compression fractures were defined as follows: localized spontaneous pain and pain on percussion of the vertebral spinous process, a bone marrow edema pattern as assessed by MRI, and reduced vertebral height on radiography. Two radiologists independently reviewed imaging findings, and if their opinions did not agree, the final diagnosis was determined after consultation between both radiologists.

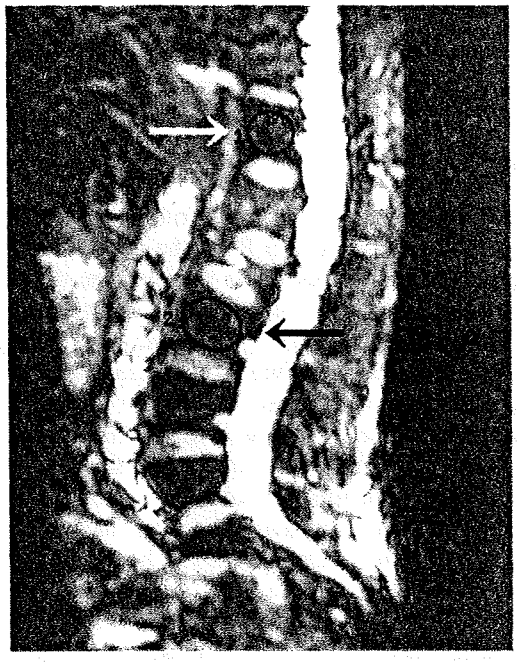

Fig. 1. User-defined ROI. Mid-sagittal diffusion-weighted image before PVP in a 64-year-old woman with L1 and L2 compression fractures. Two days after, PVP was performed on L1 and L2, so target vertebral bodies were Th12 and L3. The large fitting circle and ellipse were positioned centrally on Th12 and L3 (arrow).

Evaluated items and statistics

Relationships between preoperative ADC and new compression fractures were examined from two perspectives. By measuring ADC for each adjacent vertebral body, the ADC of vertebral bodies with a new compression fracture within 1 month and those without a new compression fracture was compared. In addition, mean ADC of adjacent vertebral bodies per patient was calculated, and ADC of patients with new compression fractures within 1 month and patients without new compression fractures was compared. Furthermore, changes in ADC before and after PVP were examined. In cases with one adjacent vertebra that met with inclusion criteria, the ADC of the vertebra was used as the mean ADC of adjacent vertebral bodies, and with more than one more adjacent vertebra, the mean ADC of the adjacent vertebrae was used.

Two-sample t tests were used to compare ADCs between vertebral bodies with new compression fractures within 1 month of PVP and those without, and to compare ADCs between patients with new compression fractures within 1 month of PVP and those without. One-sample t tests were used to compare ADCs before and after PVP. Values of $P < 0.05$ were considered statistically significant.

Results

Within 1 month of PVP, a new compression fracture had developed in seven vertebral bodies in seven of the 25 patients (28.0%). Of the seven new fractures, six were adjacent-level fractures (24%), while one was a non-adjacent-level fracture (4%). No new compression fractures were seen within 1 month of PVP in the other 18 patients (Table 2).

Mean preoperative ADC for the six adjacent vertebral bodies with new compression fractures was 0.55×10^{-3} mm^2/s (range 0.36–1.01×10^{-3} mm^2/s), and that of the 43 adjacent vertebral bodies without new compression fractures 0.20×10^{-3} mm^2/s (range 0–0.98×10^{-3} mm^2/s). This difference was statistically significant ($P < 0.001$; Fig. 2). Mean preoperative ADC for the six patients with new compression fractures was 0.55×10^{-3} mm^2/s (range 0.21–1.01×10^{-3} mm^2/s), and that for the 19 patients without new compression fractures 0.17×10^{-3} mm^2/s (range 0.01–0.43×10^{-3} mm^2/s). A statistically significant difference was again identified between the two groups ($P < 0.001$; Fig. 3).

Mean ADC for adjacent vertebral bodies was 0.24×10^{-3} mm^2/s (range 0–1.01×10^{-3} mm^2/s)

Table 2. New compression fractures within 1 month.

Patient	Sex	Age, years	PVP performed on vertebral bodies	Analyzed vertebral bodies	Newly developed vertebral body fracture after PVP
A	M	76	L2, L3	L1, L4	L1: new fracture
B	F	66	TH12, L1, L2, L3	Th11, L4	L4: new fracture
C	F	74	Th11, Th12, L1	Th10, L2	L2: new fracture
D	F	76	Th6, Th8	Th9	Th9: new fracture
E	F	79	Th12	Th11, L1	L1: new fracture
F	M	66	L1	Th12, L2	Th12: new fracture
G	M	54	L1	Th12, L2	
H	F	70	Th12	Th11, L1	
I	F	69	Th12, L1, L2	Th11, L3	
J	F	64	L1, L2	L3	
K	F	80	Th12, L3	L1	
L	F	76	L1, L4	L2, L3, L5	
M	F	69	Th12, L1, L3	L2, L4	
N	F	72	L3	L2, L4	
O	F	70	L4, L5	L3	
P	F	71	L1, L2, L3	Th12, L4	
Q	F	84	L3	L2, L4	
R	F	76	Th11, Th12, L1, L2	Th10	
S	F	78	L1, L4, L5	Th12, L2, L3	
T	F	63	Th12	Th11, L1	
U	F	79	Th11, Th12, L3	L1, L2, L4	
V	F	71	Th12, L4, L5	Th11, L3	
W	F	71	Th12, L1, L3	Th11, L2, L4	
X	F	78	Th9, Th12, L1	Th11, L2	L4: new fracture not adjacent vertebral body
Y	F	74	Th12, L1	Th11, L2	
(n=25)	3 M, 22 F	72.2±6.5	56 (20 Th, 36 L)	49 (16 Th, 33 L)	7 (2 Th, 5 L)

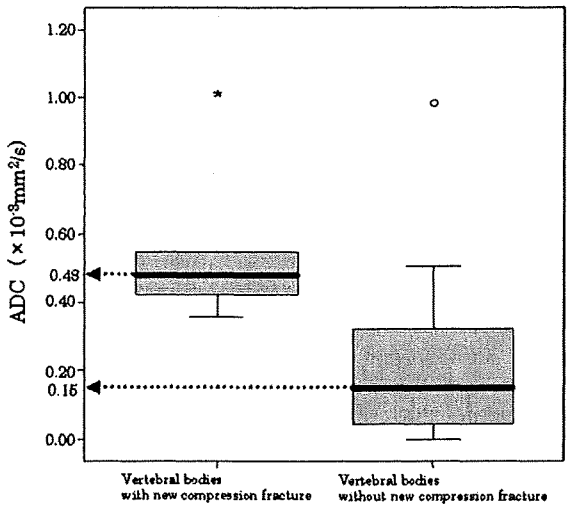

Fig. 2. Mean ADC for individual vertebrae before PVP. Mean ADC for vertebral bodies with a new compression fracture was 0.55×10^{-3} mm^2/s (range 0.36–1.01×10^{-3} mm^2/s, median value 0.48×10^{-3} mm^2/s). In contrast, mean ADC for vertebral bodies without a new compression fracture was 0.20×10^{-3} mm^2/s (range 0–0.98×10^{-3} mm^2/s, median value 0.15×10^{-3} mm^2/s). Statistically significant differences were noted between the two groups (P <0.001).

before PVP and 0.24×10^{-3} mm^2/s (range 0–0.82×10^{-3} mm^2/s) after PVP, and no statistically significant difference was apparent.

Discussion

According to past studies that followed patients for more than 6 months after PVP, the incidence of new compression fractures varies widely from 0 to 50% (4, 16–20). Uppin et al. reported an incidence of 12.5%, and noted that 67% of these were adjacent-level fractures (4). Two hypotheses have been proposed for the onset of a new compression fracture: 1) onset of a new compression fracture is unrelated to PVP (21); and 2) onset of a new compression fracture in adjacent vertebral bodies is high because cement injection increases the strength of the treated vertebral bodies, resulting in a relative weakening of untreated vertebral bodies (22, 23). Furthermore, new compression fractures tend to occur at adjacent levels (2–4) relatively soon after PVP (4). However, whether new compression fractures are attributable to PVP or a natural course of osteoporosis remains unclear at present.

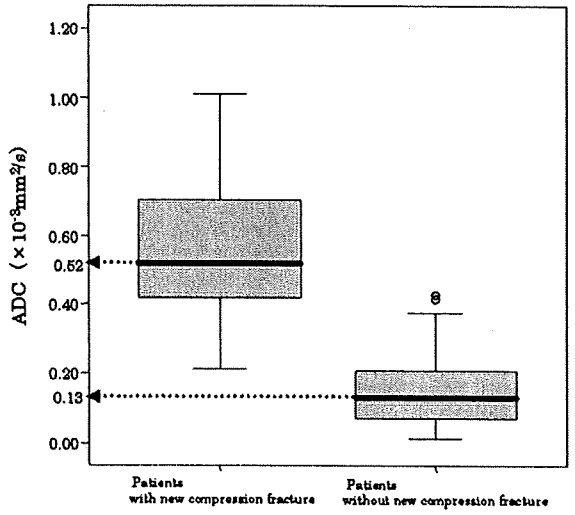

Fig. 3. ADC for each patient before PVP. Mean ADC for the six patients with new compression fractures was 0.55×10^{-3} mm^2/s (range 0.21–1.01 $\times 10^{-3}$ mm^2/s, median value 0.52×10^{-3} mm^2/s), while that for the 19 patients without new compression fractures was 0.17×10^{-3} mm^2/s (range 0.01–0.43 $\times 10^{-3}$ mm^2/s, median value 0.13×10^{-3} mm^2/s). Statistically significant differences existed between the two groups ($P < 0.001$).

In our study, new compression fractures were seen in seven of the 25 patients (28%). Since patients were followed for 1 month, this figure was higher than reported in previous studies (4, 16–20). Reasons for this could have been that one study defined new fractures as compression fractures seen on plain radiography taken when patients returned to hospital with recurrent back pain following PVP (4), while some prospective follow-up studies (3, 24) based diagnoses solely on conventional radiography. In the present study, the definition of a new compression fracture emphasized clinical features: even if the degree of decrease in vertebral height on plain radiography was minute, patients were diagnosed with new compression fractures if pain on percussion of the vertebral spinous process and a bone marrow edema pattern as assessed by MRI were observed. These criteria were utilized to ascertain whether additional PVP was required at the time of assessment.

Prophylactic PVP is currently contraindicated for vertebral bodies without compression fractures (25), but research on prophylactic PVP has been conducted in recent years (26, 27). If the risk of a new compression fracture can be evaluated accurately and vertebral bodies at higher risk for compression fractures can be identified, use of prophylactic PVP may be justified. At present, PVP is performed to treat vertebral bodies with compression fractures, and is thus only performed on patients with an existing compression fracture. According to one study, up to 25% of patients with compression fractures develop new compression fractures within 1 year (12). As mentioned above, new compression fractures after PVP are likely to occur at adjacent levels, and vertebral bodies adjacent to vertebral bodies treated by cement injection thus appear to be at higher risk for new compression fracture.

Diffusion in a microscopic sense is a phenomenon dependent on the random or Brownian motion of individual molecules. MRI can be made sensitive to diffusion of tissue water molecules, when very strong bipolar gradient pulses are inserted into either a spin-echo pulse sequence (STEJSKAL and TANNER technique) (28) or a gradient-echo pulse sequence (10). As far as the random motion of water molecules is concerned, because size and direction change markedly depending on temperature and surrounding environment, microscopic cellular conditions can be ascertained by examining the diffusion of water molecules. The number of protons gives the intensity of the MRI signal, and their motion because of thermal diffusion gives the ADC. In normal vertebral bodies, barely any mobile free water is present in the interstitial space. As a result, with the echo-planar imaging (EPI) pulse sequence used in the present study, fat signals are suppressed to resolve the issue of chemical-shift artifacts. Subsequently, in normal vertebral bodies, the number of mobile protons generating signals on MRI is very low, resulting in very low ADC. Conversely, high ADC indicates large numbers of mobile protons, suggesting mobile free water in the interstitial space, or tumor cells in bone marrow. The ADC of vertebral bodies with benign fractures is higher than that of normal vertebral bodies because of an increase in interstitial space caused by edema or hemorrhage (10, 12, 14). MIKAMI et al. reported that an area with exudate and neutrophil infiltration in a vertebral body was recognized as a high ADC area in their animal experiments of bone marrow inflammation (29). Since the amount of mobile free water is likely to be high in vertebral bodies about to develop compression fractures, measuring ADC in vertebral bodies seems likely to offer a reasonable assessment of the likelihood of compression fractures. We set the b value to 1000 s/mm^{-2}. Although the optimal b value for vertebral DWI has yet to be determined, diffusion has greater influence at higher b values such as 1000 s/mm^{-2} (12).

If PVP itself were involved in the onset of new adjacent-level fractures, the significance of preventative PVP would clearly be lost. Therefore, to ascertain the effects of PVP on adjacent vertebral bodies, ADCs were compared before and after PVP. The results showed no statistically significant differences in ADC before and after the procedure. From these results, PVP does not induce inflammation because of no increase of mobile free water. However, the influence of PVP on an adjacent vertebral body also includes biomechanical factors, and we were not able to conclude that PVP itself does not affect the incidence of new adjacent vertebral compression fractures.

In the present study, ADC was only measured using the EPI pulse sequence in DWI. EPI allows DWI to be performed in a short period of time, and since all necessary data for a single image can be gathered from a single radiofrequency excitation, the effects of motion artifacts are low. However, EPI is very sensitive to susceptibility effects, which therefore represent a major concern. Reducing these artifacts requires use of a high-receiver bandwidth or radiofrequency (RF) coil with cylindrical geometry, such as a body coil (10). However, the present study used a quadrature detection thoracolumbar spine coil with a moderate receiver bandwidth. Using EPI, susceptibility artifacts are substantially suppressed by using shorter time for signal sampling. This can be achieved by the parallel imaging technique. However, we did not use parallel imaging. Sufficient measures against susceptibility effects were thus not enforced, and this represents a significant limitation to the present study. Future investigations will require measurement of ADC using line scanning.

The results of this study suggest the possibility of predicting compression fractures of vertebral bodies adjacent to vertebral bodies injected with cement substance, and contribute toward clarifying the significance of prophylactic PVP. However, as only adjacent vertebral bodies were examined in a small number of subjects, these findings alone do not justify the introduction of preventative PVP.

In conclusion, the ADC of adjacent vertebral bodies as assessed by diffusion-weighted imaging before PVP might be a predictor for a new compression fracture following PVP.

Acknowledgements

We are grateful to members of the MRI group at Kansai Medical University for valuable assistance.

References

1. Galibert P, Deramond H, Rosat P, Le Gars D. Preliminary note on the treatment of vertebral angioma by percutaneous acrylic vertebroplasty [in French]. Neurochirugie 1987;33:166–8.
2. Grados F, Depriester C, Cayrolle G, Hardy N, Deramond H, Fardellone P. Long-term observations of vertebral osteoporotic fractures treated by percutaneous vertebroplasty. Rheumatology 2000;39:1410–4.
3. Perez-Higueras A, Alvarez L, Rossi RE, Quinones D, Al-Assir I. Percutaneous vertebroplasty: long-term clinical and radiological outcome. Neuroradiology 2002;44: 950–4.
4. Uppin AA, Hirsch JA, Centenera LV, Pfiefer BA, Pazianos AG, Choi IS. Occurrence of new vertebral body fracture after percutaneous vertebroplasty in patients with osteoporosis. Radiology 2003;226:119–24.
5. Evans AJ, Jensen ME, Kip KE, DeNardo AJ, Lawler GJ, Negin GA, et al. Vertebral compression fractures: pain reduction and improvement in functional mobility after percutaneous polymethylmethacrylate vertebroplasty – retrospective report of 245 cases. Radiology 2003;226:366–72.
6. Heini PF, Walchli B, Berlemann U. Percutaneous transpedicular vertebroplasty with PMMA: operative technique and early results. Eur Spine J 2000;9:445–50.
7. Hodler J, Peck D, Gilula LA. Midterm outcome after vertebroplasty: predictive value of technical and patients-related factors. Radiology 2003;227:662–8.
8. Kallmes DF, Jensen ME. Percutaneous vertebroplasty. Radiology 2003;229:27–36.
9. Mathis JM, Barr JD, Belkoff SM, Barr MS, Jensen ME, Deramond H. Percutaneous vertebroplasty: a developing standard of care for vertebral compression fractures. Am J Neuroradiol 2001;22:373–81.
10. Chan JHM, Peh WCG, Tsui EYK, Chau LF, Cheung KK, Chan KB, et al. Acute vertebral body compression fractures: discrimination between benign and malignant causes using apparent diffusion coefficients. Br J Radiol 2002;75:207–14.
11. Herneth AM, Philipp MO, Naude J, Funovics M, Beichel RR, Bammer R, et al. Vertebral metastases: assessment with apparent diffusion coefficient. Radiology 2002;225:889–94.
12. Lindsay R, Silverman SL, Cooper C, Hanley DA, Barton I, Broy SB, et al. Risk of new vertebral fracture in the year following a fracture. JAMA 2001;285:320–1.
13. Maeda M, Sakuma H, Maier SE, Takeda K. Quantitative assessment of diffusion abnormalities in benign and malignant vertebral compression fractures by line scan diffusion-weighted imaging. Am J Roentgenol 2003;181: 1203–9.
14. Zhou XJ, Leeds NE, McKinnon GC, Kumar AJ. Characterization of benign and metastatic vertebral compression fracture with quantitative diffusion MR imaging. Am J Neuroradiol 2002;23:165–70.
15. Burdette JH, Elster AD, Ricci PE. Calculation of apparent diffusion coefficients (ADCs) in brain using two-point and six-point methods. J Comput Assist Tomogr 1998;22:792–4.
16. Barr JD, Barr MS, Lemley TJ, McCann RM. Percutaneous vertebroplasty for pain relief and spinal stabilization. Spine 2000;25:923–8.

17. Cortet B, Cotton A, Boutry N. Percutaneous vertebroplasty in the treatment of osteoporotic compression fractures: an open prospective study. J Rheumatol 1999; 26:2222–8.
18. Cyteval C, Sarrabere MP, Roux JO, Thomas E, Jorgensen C, Blotman F, et al. Acute osteoporotic vertebral collapse: open study on percutaneous injection of acrylic surgical cement in 20 patients. Am J Roentgenol 1999;173:1685–90.
19. Jensen ME, Evanas AJ, Mathis JM, Kallmes DF, Cloft HJ, Dion JE. Percutaneous methylmethacrylate vertebroplasty in the treatment of osteoporotic vertebral body compression fractures: technical aspect. Am J Neuroradiol 1997;18:1897–904.
20. Zoarski GH, Snow P, Olan WJ. Percutaneous vertebroplasty for osteoporotic compression fractures: quantitative prospective evaluation of long-term outcomes. J Vasc Interv Radiol 2002;13:139–48.
21. Jensen ME, Kallmes DF, Short JG. Percutaneous vertebroplasty does not increase the risk of adjacent level fracture: a retrospective study. In: Proceedings of the American Society of Neuroradiology, Atlanta, GA, April 3–8, 2000.
22. Berlemann U, Ferguson SJ, Nolte LP, Heini PF. Adjacent vertebral failure after vertebroplasty: a biomechanical investigation. J Bone Joint Surg Br 2002;84: 748–52.
23. Polikeit A, Norte LP, Ferguson SJ. The effect of cement augmentation on the load transfer in an osteoporotic functional spinal unit: finite-element analysis. Spine 2003;28:991–6.
24. Legroux-Gerot I, Lormeau C, Boutry N, Cotton A, Duquesnoy B, Cortet B. Long-term follow-up of vertebral osteoporotic fractures treated by percutaneous vertebroplasty. Clin Rheumatol 2004;23:310–7.
25. Barr JD, Mathis JM, Barr MS, Denardo AJ, Dion JE, Guterman LR, et al. Standard for the performance of percutaneous vertebroplasty. In: American College of Radiology Standards 2000–2001. Reston, VA: American College of Radiology; 2000. p. 441–8.
26. Sun K, Liebschner MA. Biomechanics of prophylactic vertebral reinforcement. Spine 2004;29:1428–35.
27. Higgins KB, Harten RD, Langrana NA, Reiter MF. Biomechanical effects of unipedicular vertebroplasty on intact vertebrae. Spine 2003;28:1540–7.
28. Stejskal EO, Tanner JE. Spin diffusion measurements: spin echoes in the presence of time-dependent field gradient. J Chem Phys 1965;42:288–92.
29. Mikami M. Application of diffusion-weighted MR imaging to the diagnosis of bone metastasis: a fundamental study using rabbit bone tumor model. Nippon Igaku Hoshasen Gakkai Zasshi 2004;64:107–13.

The British Journal of Radiology, 82 (2009), 249–253

SHORT COMMUNICATION

Cerebral microembolisation during radiofrequency ablation of lung tumours: detection by carotid duplex ultrasound

[1]N TANIGAWA, MD, PhD, [1]S KARIYA, MD, PhD, [1]H KOJIMA, MD, [2]A KOMEMUSHI, MD, PhD, [1]Y SHOMURA, MD, PhD, [2]K IKEDA, MD, PhD, [1]N OMURA, MD, [1]T TOKUDA, MD, [1]M MAEHARA, MD, [1]J TERADA, MD and [1]S SAWADA, MD, PhD

[1]*Department of Radiology, Kansai Medical University Hirakata hospital, 2-3-1 Shinmachi, Hirakata, Osaka, 573-1191 and* [2]*Department of Radiology, Kansai Medical University Takii Hospital, 10-15 Fumizono, Moriguchi, Osaka, 570-0074, Japan*

ABSTRACT. The aim of this study was to investigate the appearance of microbubbles during radiofrequency ablation (RFA) of lung tumours. Eight consecutive patients (mean age, 73.1 years; 3 men and 5 women; 10 malignant lesions; mean lesion size, 24.8 mm) who underwent RFA of lung tumours using internally cooled single electrodes were enrolled. During the RFA procedure, the right internal carotid artery was continuously monitored by duplex ultrasound. High-intensity transient signals (HITS) that occurred in the Doppler blood flow waveform were taken to indicate microbubbles. 21 RFA applications were performed for the 10 lesions. HITS were observed in 19 of 21 RFA applications; the mean frequency in a single application was 10 ± 13.3. A statistical correlation was seen between the duration of energy deposition and the number of HITS, and between tumour size and the number of HITS. Microbubbles were detected in all patients in the late phase of the first session of RFA.

Received 2 January 2008
Revised 1 May 2008
Accepted 7 May 2008

DOI: 10.1259/bjr/10127675

In radiofrequency ablation (RFA) treatment, heat is generated in the non-insulated portion of the electrode by dielectric heating caused by radiofrequency. The heating results in coagulation necrosis of the target tissue. The circumstances of heat generation vary according to the anatomical environment of the tissue surrounding the probe tip, *e.g.* differences in the vasculature and tissue resistance and in the shape of the electrode.

Microbubbles are known to form during RFA of the liver [1–4]. When they do form during RFA of lung tumours, these microbubbles enter the pulmonary veins, and the emboli then continue into the systemic circulation via the left heart. It has been suggested that these emboli may also enter the cerebral circulation and cause cerebral complications, specifically microembolism. Microbubble formation has also been reported to occur during RFA of lung tumours, and the effect of microbubbles on the brain has been investigated by CT and MRI [5, 6]. We therefore designed a prospective study to investigate the number of microbubbles per minute during pulmonary RFA using internally cooled electrodes.

Address correspondence to: Noboru Tanigawa, Department of Radiology, Kansai Medical University Hirakata hospital, 2-3-1Shinmachi, Hirakata, Osaka, 573-1191, Japan. E-mail: tanigano@hirakata.kmu.ac.jp

Methods and materials

Patients

The study was conducted in accordance with the Declaration of Helsinki and written informed consent was obtained from all patients prior to treatment. Subjects comprised 8 consecutive patients (mean age, 73.1 years; range, 64–89 years; 3 men and 5 women; 10 lesions) who underwent RFA treatment of lung tumours. The underlying disease was primary lung cancer in four patients and metastatic lung cancer in four patients, with the primary cancers in these patients being gastric cancer, maxillary cancer, hepatocellular carcinoma and colon cancer. One primary lung cancer patient and the patient with lung metastasis of maxillary cancer had two lesions in both lungs; RFA was therefore performed twice, on different days. 10 treatments were performed for the 10 lesions, comprising 21 RFA sessions. A mean of 2.1 RFA sessions (range, 1–4 sessions) were performed for each lesion.

RFA procedure

All procedures were performed under conscious sedation. As pre-medication, 0.5 mg of atropine sulphate (Tanabe, Osaka, Japan), 25 mg of hydroxyzine hydrochloride (Pfizer Japan, Tokyo, Japan), and 10 mg of morphine hydrochloride (Sankyo, Tokyo, Japan) were administered by intramuscular injection 30 min before the procedure.

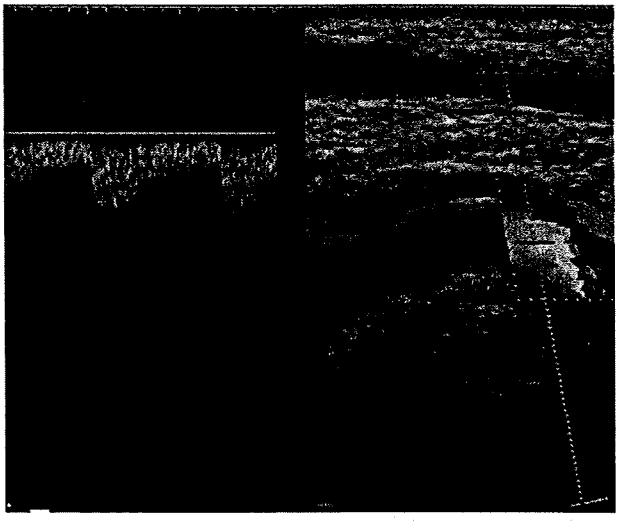

Figure 1. Duplex ultrasound image obtained during radiofrequency ablation.

The electrode used in all cases was an internally cooled single needle. The generator used was the Cool-Tip system (Radionics, Burlington, MA), with ablation performed in impedance control mode.

Two grounding pads were attached to both thighs. Unenhanced CT imaging of the area including the lesion (slice thickness, 3 mm; interval, 3 mm) was then performed; the puncture line was visualized; and local anaesthesia was performed by administering 10 cm^3 of 1% xylocaine directly beneath the parietal pleura along the puncture line using a 22-gauge Cathelin needle (Terumo Europe, Leuven, Belgium). CT imaging was repeated with the Cathelin needle used for local anaesthesia still in place. The orientation of the Cathelin needle was determined, and a 17-gauge 15 cm internally cooled single electrode (Radionics) was then advanced to the lesion site. The location of the probe in relation to the tumour was determined by CT, and the application of current was initiated. An electrode with a 2 cm non-insulated portion was used for tumours <2 cm in diameter, and an electrode with a 3 cm non-insulated portion was used for tumours ≥2 cm in diameter.

An algorithm of energy deposition was initiated at 15–30 W and was gradually increased at a rate of 10 W min^{-1}. The endpoint of one RFA application was defined as the point at which the RFA generator output automatically stopped when the impedance increased by 20 ohm compared with the initial level. At the completion of each application, CT imaging was performed and the tumour periphery was checked for the appearance of ground-glass shadow. If no ground-glass shadow was present in the tumour periphery, the puncture needle was relocated and multiple ablations were performed. The endpoint of a single procedure was defined as the appearance of ground-glass shadow in the entire region of the tumour periphery. During the ablation procedure, output, impedance and the temperature of the tip of the electrode were continuously monitored.

Immediately after the RFA treatment, unenhanced CT imaging of all lung fields (slice thickness, 5mm; interval, 15 mm) was performed, and the presence or absence of pneumothorax was determined. For 2 h after RFA, the patient rested in the supine position and underwent nasal oxygen inhalation at a rate of 2 l min^{-1}. The chest radiograph was taken in the sitting position using a portable imaging system 2 h after the ablation procedure, and the chest radiography was performed the following day to check for pneumothorax.

Monitoring of the internal carotid artery with duplex ultrasound

During the RFA procedure, the right internal carotid artery was continuously monitored by duplex ultrasonography (Figure 1). Firstly, the internal carotid artery was identified and sample points in the carotid were established by B-mode ultrasonography (Power Vision 8000; Toshiba, Tokyo, Japan). Then, the Doppler angle was aligned to the jet and kept below 60°. The pulsed Doppler gate was positioned in the centre of the common carotid artery, approximately 1–2 cm proximal to the carotid bifurcation, and a spectral waveform was obtained. The gate size was fixed on 5 mm and the velocity range was also fixed at 53.7 cm s^{-1}. Before the radiofrequency energy deposition, the Doppler blood flow waveform was monitored to determine a baseline number of high-intensity transient signals (HITS). HITS that occurred in the Doppler blood flow waveform were taken to indicate microbubbles (Figure 2). HITS were defined as follows: (i) audible high-intensity Doppler signals of brief duration; (ii) signals that were predominantly unidirectional; and (iii) signals occurring singly or, if more than one, randomly throughout the cardiac cycle.

Using a linear 7 MHz probe, monitoring was performed continuously from the time at which RFA output was initiated until 1 min after output was stopped. A super VHS video recording of the online screen was obtained for reading and analysis. HITS were confirmed

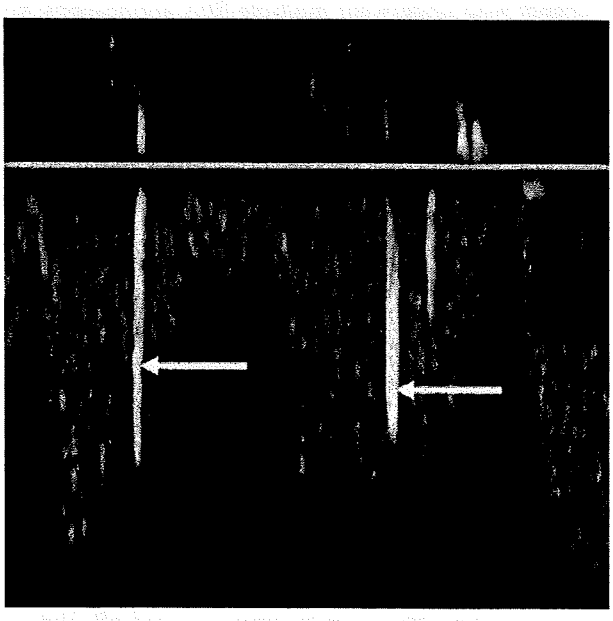

Figure 2. Pulse wave image obtained radiofrequency ablation. Visible vertical spikes (white arrows) indicating microemboli were seen.

both visually and auditorily, and the timing and frequency of their occurrence were recorded.

Data analysis

We recorded the site of RFA treatment, maximum tumour diameter, ablation time for each application, and maximum output. If multiple applications were performed for a single treatment, we also recorded whether the needle position was changed between the initial and subsequent applications.

Continuous observation for HITS was carried out from the initiation to completion of ablation in each RFA application. The number of HITS in each 1-min interval was recorded, and the total number of HITS per application was examined.

Statistical analysis

The presence or absence of a correlation between tumour size and HITS frequency and between maximum output and HITS frequency was determined using Pearson's correlation coefficient. For patients in whom RFA was performed twice at the same site for a single lesion with no change in the location of the radiofrequency probe, the difference in HITS frequency between the first and second RFA applications was tested for significance using the Wilcoxon signed-ranks test.

Results

Mean lesion size was 24.8 mm (range, 10–55 mm). For the first treatment, one patient underwent a single application, eight patients underwent two applications, and one patient underwent four applications. Among the patients who underwent multiple RFA applications, six underwent two applications for the same site without changing the needle position, and two had a change of needle position between the two applications. The remaining patient underwent four applications for the same tumour, with the same needle position used for the first and second applications; the needle position was changed for the third application, and this needle position was maintained in the fourth application. A single application took 14 min 45 s±0 min 45 s (range, 3 min 20 s to 47 min 12 s). Maximum radiofrequency energy output was 96.4±35.5 W (range, 50–150 W).

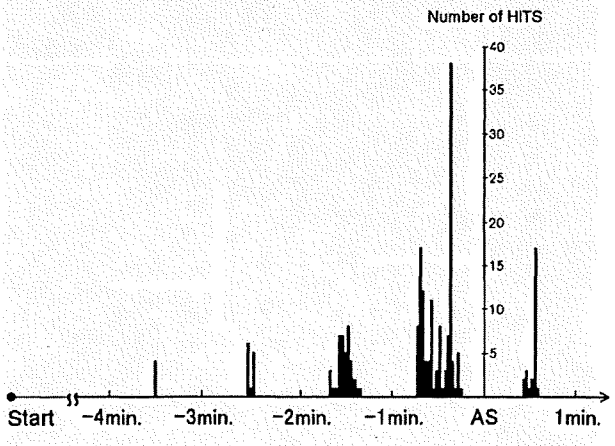

Figure 3. Graph shows the timing and frequency of high-intensity transient signals (HITS) in each case. HITS persisted for 1 min after energy was automatically shut off, and we observed a tendency towards an increasing frequency of HITS towards this shut-off. AS, automatic stop of energy deposition; Start, the start of radiofrequency energy deposition.

HITS were observed during RFA in 19 of 21 applications; the mean frequency in a single application was 10±13.3 (range, 0–60; Table 1). In the two applications in which HITS did not occur (second application of lesion 1, and second application of lesion 6), we performed the second RFA application immediately after the first one, targeting the same tumour and using the same needle position. In contrast, HITS were observed in all first RFA applications of the treatment.

The timing and frequency of HITS in each case are shown in Figure 3. HITS persisted for 1 min after the energy was automatically shut off, and we observed a tendency towards an increasing frequency of HITS towards this shut-off. On average, HITS appeared 85.5 s before energy output stopped. Furthermore, as the end of the RFA application approached, we usually identified more occurrences of HITS (Figure 3). A statistical correlation was seen between the duration of energy deposition and the number of HITS (r=0.545, p=0.0095). A statistical correlation also was found between tumour size and the number of HITS (r=0.848, p=0.001). In patients who underwent multiple RFA applications at the same site, a statistically significant difference was seen between the initial application and subsequent applications with respect to the frequency of HITS (p=0.0352).

Discussion

Microbubbles can also occur during RFA of lung tumours, and to date there have been two reports of microbubble detection during this procedure [5, 6]. If they do develop, these microbubbles enter the pulmonary veins and continue into the systemic circulation via the left heart.

To detect microbubbles in the cerebral circulation, we used duplex ultrasound to ascertain HITS in the internal carotid artery. Normally, HITS monitoring of the carotid artery is used for the detection of microbubbles, and HITS are considered to represent intravascular air bubbles or thrombi [7–9]. In the present investigation, HITS were detected in 19 of 21 RFA applications, occurring in the initial RFA application in all of the patients. Thus, the findings indicated that microbubbles occurred in all patients who underwent RFA of lung tumours, as is the case with RFA of liver tumours, and that the microbubbles may have entered the systemic and cerebral circulation from the pulmonary veins via the left heart. The number of patients was small but the total number of HITS might be much greater if the true probability of HITS in all arteries was estimated. Moreover, the microbubbles tended to occur immediately before output was automatically stopped owing to an increase in impedance. This indicated that the

Table 1. A summary of results

Lesion no.	Maximum diameter (mm)	Application no.	Electrode position of each RFA application	Duration of RFA	Maximam power (watt)	Total number of HITS
1	15	1st		9 min 45 s	80	8
		2nd	Same[a]	6 min 6 s	70	0
2	30	1st		16 min 12 s	130	19
		2nd	Different[b]	17 min 43 s	130	12
3	18	1st		5 min 5 s	60	10
		2nd	Same	3 min 50 s	50	4
4	28	1st		47 min 12 s	108	23
5	20	1st		3 min 20 s	70	1
		2nd	Same	11 min 29 s	50	4
		3rd	Different	6 min 45 s	50	8
		4th	Same	9 min 9 s	50	3
6	28	1st		15 min 15 s	130	11
		2nd	Same	17 min 00 s	130	0
7	55	1st		21 min 3 s	140	19
		2nd	Different	27 min 27 s	150	60
8	10	1st		11 min 14 s	70	12
		2nd	Same	10 min 35 s	70	1
9	30	1st		18 min 28 s	126	10
		2nd	Same	17 min 45 s	130	2
10	25	1st		20 min 12 s	110	1
		2nd	Same	14 min 00 s	120	2

RFA, radiofrequency ablation; HITS, high-intensity transient signals.
[a]Same means the same electrode position as the previous ablation.
[b]Different means a different electrode position from the previous RFA application.

microbubbles occurred during the time that the temperature increase in the periphery of the radiofrequency probe was at its peak. HITS occurred for all but 2 of the 22 RFA applications. Both of these applications were the second RFA application for the same tumour, performed with no change in the location of the probe from that used at the first RFA application. A possible explanation for the absence of microbubbles in these cases is that the fluid in the periphery of the radiofrequency probe may have evaporated during the first RFA application, leaving no fluid to cause microbubbles during the second application. This indicates that the HITS that we observed may have resulted from water vapour produced by vaporization of fluid in the tissues caused by the high temperature. Rose et al [5] identified vapour formation from (i) blood and water, (ii) nitrogen or nitrous oxide gas leaving solution during tissue heating, and (iii) carbon dioxide generated from charring as possible sources of microbubbles during lung RFA.

Yamamoto et al [6] monitored the internal carotid artery by Doppler ultrasound during lung RFA and observed microbubbles with brightness-mode and/or Doppler scanning in only 3 of 17 patients. We found no microbubbles with brightness-mode scanning in any of the patients examined. However, the frequency of HITS in our investigation was clearly higher than that reported by Yamamoto et al [6]. Possible explanations for this are differences in the output of the RFA generator, and in the manner in which the tissue was ablated owing to variation in the shape of the RFA needle. Yamamoto et al [6] used a 15-gauge Leveen needle, and the difference in the shape of the non-insulated portion of the radiofrequency probe tip may have resulted in a difference in the rate of tissue temperature increase and, consequently, a different form of ablation. Moreover, the mean maximum radiofrequency output was 96.4 W in our investigation and 48.7 W in the investigation of Yamamoto et al [6], a difference that may have been a cause of the discrepancy in frequency of microbubbles observed. In the present study, the number of HITS increased with the duration of radiofrequency current application. This may have resulted from the fact that the final temperature was higher with longer current application. The number of HITS also increased with tumour size, possibly because the volume of tissue in which coagulation occurred was greater, and the tissue therefore contained more fluid.

The present study had several limitations. Firstly, we did not differentiate between solid emboli and gas bubbles, and the small number of patients in this study makes it difficult to conclude that microbubbles have no effect on the cerebral circulation. Secondly, only the right internal carotid artery was examined in all patients. There is a possibility that microbubbles also flow in the left internal carotid artery, as well as in vertebral arteries. In addition, the probability of this flow might also depend upon the position of the patient during the ablation.

In conclusion, microbubbles were detected in all patients in the late phase of the first session of RFA.

References

1. Kruskal JB, Oliver B, Huertas JC, Goldberg SN. Dynamic intrahepatic flow and cellular alterations during radiofrequency ablation of liver tissue in mice. J Vasc Interv Radiol 2001;12:1193–201.
2. Livraghi T, Goldberg SN, Lazzaroni S, Meloni F, Solbiati L, Gazella GS. Small hepatocellular carcinoma: treatment with radio-frequency ablation versus ethanol injection. Radiology 1999;210:655–61.

3. Livraghi T, Goldberg SN, Lazzaroni S, Meloni F, Ierace T, Solbiati L, et al. Hepatocellular carcinoma: radio-frequency ablation of medium and large lesions. Radiology 2000;214:761–8.
4. Malone DE, Lesiuk L, Brady AP, Wyman DR, Wilson BC. Hepatic interstitial laser photocoagulation: demonstration and possible clinical importance of intravascular gas. Radiology 1994;193:233–7.
5. Rose SC, Fotoohi M, Levin DL, Harrell H. Cerebral microembolization during radiofrequency ablation of lung malignancies. J Vasc Interv Radiol 2002;13:1051–4.
6. Yamamoto A, Matsuoka T, Toyoshima M, Okuma T, Oyama Y, Hamuro M, et al. Assessment of cerebral microembolism during percutaneous radiofrequency ablation of lung tumors using diffusion-weighted imaging. AJR Am J Roentgenol 2004;183:1785–9.
7. Consensus Committee of the Ninth International Cerebral Hemodynamic Symposium. Basic identification criteria of doppler microembolic signals. Stroke 1995;26:1123.
8. Markus H, Loh A, Israel D, Buckenham T, Clifton A, Brown MM. Microscopic embolism during cerebral angiography and strategies for its avoidance. Lancet 1993;341:784–7.
9. Russell D, Madden KP, Clark WM, Sandset PM, Zivin JA. Detection of arterial emboli using Doppler ultrasound in rabbits. Stroke 1991;22:253–8.